Modeling and Simulation of An Entrained Flow Coal Gasifier

A mathematical model has been developed to simulate the Texaco downflow entrained-bed pilot-plant gasifier using coal liquefaction residues and coal-water slurries as feedstocks. This model describes the physical and chemical processes occurring in an entrained coal gasifier. The gasification kinetics describes different complex reactions occurring in the gasifier and the hydrodynamics describes mass, momentum and energy balances for solid and gas phases. Temperature, concentration and velocity profiles along the reactor height were obtained by solving the mass, momentum and energy balances. Parameter studies were made to provide a better understanding of the reactor performance for various inlet feed conditions utilizing the model.

RAKESH GOVIND and JOGEN SHAH

Department of Chemical and Nuclear Engineering
University of Cincinnati
Cincinnati, OH 45221

SCOPE

Entrained-bed gasifiers are cocurrent flow reactors in which pulverized or atomized hydrocarbons react with oxygen and steam to produce gaseous fuels. These reactors are becoming popular in the processing of coal into synthetic fuels and thermal energy since they produce higher coal gasification rates and are easier to operate than fluidized- or fixed-bed reactors. Further, due to the incineration effect they produce a product gas that is relatively free of higher hydrocarbons particularly the tarry materials.

In this paper, a mathematical model has been developed to simulate the Texaco downflow entrained-bed pilot-plant gasifier using coal liquefaction residues as feedstocks. Results of the simulation have been compared with experimental data from the gasifier.

CONCLUSIONS AND SIGNIFICANCE

The Texaco downflow pilot-plant gasifier was simulated by simultaneously solving the mass, momentum and energy balances for the solid and gas phases. Good agreement was obtained between the simulation programs and experimental results. The gas composition leaving the gasifier and the final carbon conversion depends on three essential parameters: the fuel rate, the oxygen to fuel ratio, and the steam-fuel ratio. It was found that oxygen-fuel ratio affects carbon conversion more than the steam-fuel ratio. The steam-fuel ratio significantly affects the gas product composition. The optimum oxygen-fuel ratio is between 0.8 and 0.9 to achieve 98–99% conversion. Depending on the oxygen-fuel ratio, the optimum steam-fuel ratio ranges from 0.3 to 0.6 using coal liquefaction residues as feedstocks.

INTRODUCTION

As research and development continues on entrained flow reactors, a mathematical model is necessary for gaining an insight into the influence of design variables, feed materials, and processing conditions on the reactor performance. Furthermore, such models will be necessary and powerful tools in optimizing, scaling-up and designing the process.

In an entrained flow reactor, small condensed particles (solid or liquid state) are dispersed into a moving gaseous medium thereby entraining the injected particles. This provides the largest solid-gas (or liquid-gas) reactive surface area possible and reduces the gas-phase diffusional resistances, so that rapid chemical reactions between the phases can occur.

The Texaco pilot-plant gasifier, Figure 1, is a downflow entrained-bed reactor and has been described in detail in a report by Texaco's Montebello Research Laboratory (Robin, 1976). The 152.4 cm (5 ft) diameter by 609.6 cm (20 ft) long steel vessel is divided internally into two sections. The top section (330 cm long) is lined with a special refractory material specifically designed to withstand the severe operating environment expected. In this section, combustion and gasification reactions take place. The lower section is a quench vessel. A reservoir of water is maintained in the bottom of this vessel at all times by continuous injection of cooling water. Syngas leaving the top section of the gasifier passes through a water-cooled dip tube into the water reservoir in the quench vessel. Slag, most of the soot, and unreacted hydrocarbon carried with the syngas remain in the water and are then removed. The saturated syngas is removed from the gas space above the reactor.

The pulverized coal liquefaction residue is made pumpable by melting and being kept at 204–260°C and then blending with 2–7% aromatic solvent. The molten residue, oxygen, and steam are fed through a proprietary Texaco burner into the top of the pilot-plant gasifier. All of the runs with coal liquefaction residues were conducted at a pressure of $24.31 \times 10^5 N/m^2$.

For coal-water slurry runs, the coal is mixed with water and preheated to a temperature below saturation point so that water in the slurry enters the reactor as a liquid. It has been reported that the slurry can be mixed and pumped at solid loading as high as 70%, i.e., at a water/coal ratio of 0.4 (Bissett, 1978). The operating pressure for coal-water slurry runs is about $21.28 \times 10^5 N/m^2$. Table 1 shows the ultimate analysis of fuels used in the pilot-plant runs.

Correspondence concerning this paper should be addressed to Rakesh Govind.

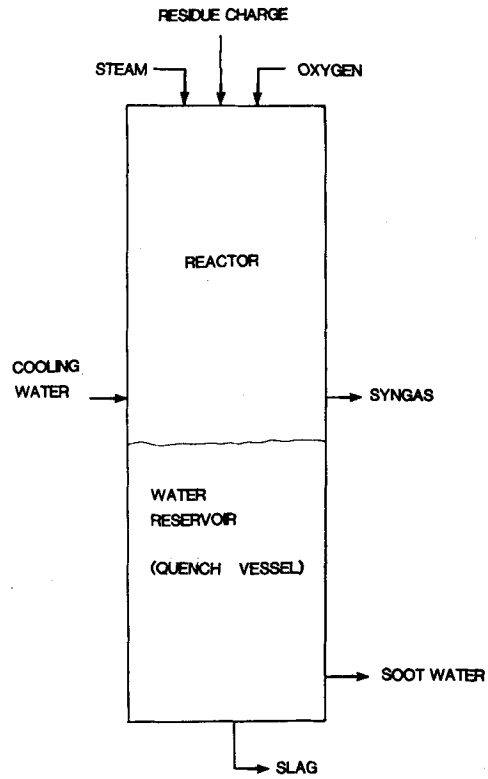

Figure 1. Texaco downflow entrained-bed pilot-plant gasifier.

Table 2 summarizes the background for the modeling of two-phase entrained-bed reactors. The mathematical model involves the simultaneous solution of mass, momentum and energy balances with the reaction kinetic equations using a stirred tank in series reactor model for both the solid and the gas phases.

Our approach is different from Kane and McCallister's (1978) and Blake's (1979) since they did not consider the chemical reaction in conjunction with reactor hydrodynamics and energy balances. Ubhayankar (1977) did not consider the momentum balance, and Wen and Chaung (1979) used the Stoke's Law approximation for the particle instead of the solid momentum balance. Sprouse (1980) and Goyal (1980) studied the hydrogasification process rather than combustion in a different type of reactor system.

REACTOR MODEL

Kinetics

In an entrained-flow reactor, the coal particles undergo major physical and chemical changes due to thermal decomposition, resulting in the evolution of gases and liquids (condensable vapors). The amount and composition of the evolved products depend on the type and size of coal and the conditions prevailing in the gasifier. The kinetics of this thermal decomposition process is quite complex and numerous mechanisms have been proposed in the literature.

Based on the chemical reactions, the gasifier can be divided into three sections:

1. Pyrolysis and volatile combustion section
2. Combustion and gasification section
3. Gasification section

Major solid gas reactions involved in coal gasification are pyrolysis, char-steam, char-carbon dioxide, char-oxygen and char-hydrogen reactions. Pyrolysis reaction which released the moisture and volatile matter in the raw fuel is usually the first to occur and the fastest among these reactions. The yields of volatiles and their composition depend not only on the volatile matter content of the raw fuel but also on the temperature, pressure and rate of heating during pyrolysis. For temperature below 1,000°C, char-steam, char-carbon dioxide and char-hydrogen reactions are usually slow and depend on the volumetric compositions. However, at temperatures above 1,200°C, the rates of these reactions, perhaps except for that of the char-hydrogen reactions, are controlled by gas-film diffusion and ash-layer diffusion. In an entrained-bed reactor, the operating temperatures are usually much higher than 1,000°C and so diffusion through the gas-film and ash-layer is the controlling factor in the gasification. Since the particle loading in an entrained-bed gasifier is small (less than 1% of the reactor volume), particle collisions are unlikely to be frequent and the ash layer formed can be assumed to remain on the fuel particle during the reaction. It is thus unreasonable to assume that the reaction rates may be estimated by the unreacted-core shrinking model for an entrained-bed gasifier. The kinetics of each reaction has been discussed in the following section.

Pyrolysis and Volatile Combustion

The input fuel, coal and coal liquefaction residues, used in an entrained-bed system, are polymeric compounds consisting of C, H, O, N, S and ash. When heated to high temperatures, it decomposes and produces volatiles which consist of a mixture of combustible gases, (CO, H_2, CH_4), carbon dioxide, Hydrogen Sulphide, Nitrogen and tar. A large amount of heat is produced in the gas phase, by the burning of the combustible volatiles, which heats the solid fuel rapidly to the pyrolysis temperature.

Rates of *coal pyrolysis* in an inert atmosphere have been investigated by many researchers (Bazioch and Hawksley, 1970; Anthony et al., 1976):

Reaction

$$C_{\alpha_i}H_{\beta_i}O_{\gamma_i}N_{\delta_i}S_{\epsilon_i}A \xrightarrow[\Delta]{} C_{\alpha}H_{\beta}O_{\gamma}N_{\delta}S_{\epsilon}A + \text{Volatiles} \quad (1)$$

Kinetic Equations

$$\frac{dV}{dt} = K(V^* - V) \quad (2)$$

$$K = K_0 \exp(-E/RT) \quad (3)$$

$$\frac{dV}{dt} = 1.14 \times 10^5 \exp(-8{,}900/T_c)\cdot(V^* - V) \quad (4)$$

$$\Delta V = VM_0(1 - c)(1 - \exp(-A(\exp(-B/T))t)) \quad (5)$$

$$\Delta W = QVM_0(1 - c)(1 - \exp(-A(\exp(-B/T))t)) \quad (6)$$

$$V^* = V^*_{nr} + V^{**}_r/(1 + 0.56\,P_t) \quad (7)$$

TABLE 1. ANALYSIS OF FEEDSTOCK USED IN TEXACO'S PILOT-PLANT TESTS*

Feedstock Source and Run No.	Dry Fuel Analysis, wt.% C	H	N	S	O	Ash	Cl
H-coal residue from Illinois No. 6 coal for run I-1	74.05	6.25	0.71	1.77	1.32	15.53	0.37
H-coal residue from Illinois No. 6 coal for run I-2	73.04	5.82	0.73	1.37	1.70	16.83	0.48
H-coal residue from Wyodak coal for run W-1	78.37	5.79	0.92	0.07	3.70	11.05	0.08
SRC-II vacuum flash drum bottoms	64.90	3.65	1.25	2.96	1.70	25.54	—
Exxon DSP vacuum tower bottoms	70.74	4.67	1.18	2.74	3.95	16.72	—
Western coal used in coal-water slurry runs	74.56	5.31	0.99	0.46	11.47	7.20	—
Eastern coal used in coal-water slurry runs	72.72	5.03	1.40	2.99	9.13	8.73	—

TABLE 2. BACKGROUND FOR MODELING OF TWO-PHASE ENTRAINED-BED REACTORS

Author	Reactor Simulated	Kinetics	Mass Balance	Momentum Balance	Energy Balance	Comments
Ubhayakar (1977)	MHD power generation plant	Devolatilization, gas-phase reactions, thermal cracking, constant particle size	Mass rate of production & volatiles, of remaining solids	Not considered	Thermal Energy	One-dimensional flow, unsteady-state, exponential *mixing* relationship, plug-flow model
Kane & McCallister (1978)	—	Not considered	Continuity Equation	Equation of motion for radial, axial and circumferential direction	Mechanical energy balance	Multidimensional flow, unsteady-state, dimensionless equations are prepared, and scale-up techniques were devised.
Wen and Chaung (1979)	Texaco gasifier	Devolatilization, char-O_2, char-H_2, char-CO_2, char-H_2O, water-gas shift	Differential equation relating reaction rate	Stoke's law is assumed for solids, exponential expression for velocity	Thermal energy balance	One-dimensional flow, steady-state, stirred-tank plug-flow model
Blake (1979)	Similar reactor system	Not considered	Continuity equations for both phases	Multidimensional momentum balance	Multidimensional mechanical balance	Multidimensional, two-phase, turbulent model, unsteady-state, nonreactive flow
Sprouse (1980)	Rockwell Int. FHP reactor	Chemistry of coal particle, devolatilization, and hydrogasification	Differential equation relating reaction rate	Equation of motion, drag force included	Mechanical energy balance	One-dimensional flow, steady-state, plug-flow, boundary layer considered
Goyal (1980)	Cities Service R&D Co.'s bench-scale reactor	Johnson's hydropyrolysis model used	Continuity equations for both phases	Mixture momentum balance was used, drag force included	Thermal energy balance considered	One-dimensional flow, steady-state, plug-flow, a model for hydrogasifier

V^*_{nr}
= potential ultimate yield of volatiles at pressure >100 atm,

V^{**}_r
= portion of volatile yield that exceeds V^*_{nr} at pressures <0.001 atm

$$V^* = V^* \text{ (at 1 atm)} \cdot (1 - a \ln P_t) \quad (8)$$

$a \simeq 0.066$ for bituminous coal $0.1 \leq$ total pressure ≤ 50 atm

Volatile Combustion

$$CO + \tfrac{1}{2}O_2 \rightarrow CO_2 \quad (9)$$

$$H_2 + \tfrac{1}{2}O_2 \rightarrow H_2O \quad (10)$$

$$CH_4 + \tfrac{3}{2}O_2 \rightarrow CO_2 + 2H_2O \quad (11)$$

$$\text{Hydrocarbons} + O \rightarrow CO_2 + x\,H_2O \quad (12)$$

(assumed C_6H_6)

Equation 4 predicts a higher pyrolysis rate than most other existing data. Experimental data by Loison and Chauvin (1964), Figure 2, are used to predict the volatile product composition. It has been assumed that, during pyrolysis, the relative compositions of the product gases are the same as obtained from Figure 2. Note that in Figure 2 the yield of hydrogen is independent of the proximate volatile matter content. Based on information on the amount of hydrogen, the ratio of CO/CO_2 and H_2O/CO_2 obtained from Figure 2 together with the material balance on different elements, the product distribution for the pyrolysis process is estimated. The volatile production rate from Eq. 4 is then matched with the product distribution assuming that the composition of the volatile product is independent of the rate.

It is important to note that we have used experimental data of Loison and Chauvin (1964) for coal liquefaction residues, since these residues are polymeric compounds of C, H, N, O and S, just like coal, and the data are applicable with the appropriate volatile content for the residue.

Further the pyrolysis reaction occurs first and is the fastest reaction. The temperature rises very quickly during the pyrolysis reaction and the reaction is completed in a very short length (about 10 cm) as compared to the total reactor length of 330 cm. Hence the final carbon conversion is not very sensitive to the pyrolysis rate.

Char-Gas Reactions

In an entrained-bed gasifier, most char-gas reactions can be considered as surface reactions because of high operating temperatures (above 1,000°C). Since the system is very dilute, particle-particle interaction is neglected; therefore, the ash layer formed can be assumed to remain on the fuel particle during the reaction. The unreacted-core shrinking model proposed by Wen et al. (1968) is used to estimate the solid-gas reaction rates. In this model effects

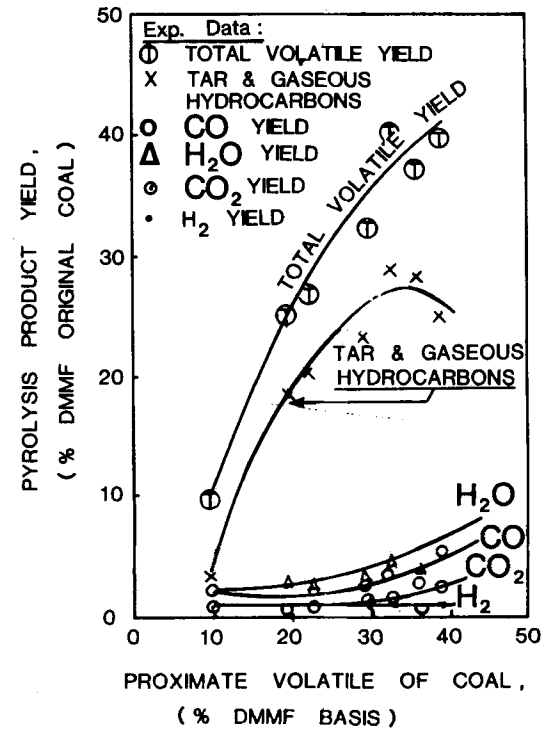

Figure 2. Product yield of coal pyrolysis (Loison and Chauvin, 1964): at 10^3 °C/s to 1,050°C.

of ash layer diffusion, gas film, diffusion and chemical reaction are considered. The overall rate can be expressed as follows,

$$\text{Rate} = \frac{1}{\frac{1}{K_{\text{diff}}} + \frac{1}{K_{\text{ash}}}\left(\frac{y-1}{y}\right) + \frac{1}{y^2 K_s}} \cdot (P_1 - P_1^*) \quad (13)$$

where

$$y = \frac{r_c}{R_p} \quad (14)$$

The ash diffusion constant, K_{ash}, is estimated by a correlation suggested by Wen et al. (1968):

$$K_{\text{ash}} = K_{\text{diff}} \epsilon_1^{2.5} \quad (15)$$

The specific char-gas reactions have been investigated by Wen and Dutta (1978), Field et al. (1967), Dobner (1976), Dutta et al. (1977), and Wen (1978).

Char-Oxygen Reaction

$$\text{Carbon} + 1/\phi\ O_2 \rightarrow 2(1 - 1/\phi)CO + (2/\phi - 1)CO_2 \quad (16)$$

$$C_\alpha H_\beta O_\gamma N_\delta S_\epsilon A + \left(\frac{\alpha}{\phi} - \frac{\gamma}{2} + \frac{\beta}{2} - \epsilon\right) O_2 \rightarrow 2(1 - 1/\phi)\alpha CO + (2/\phi - 1)\alpha CO_2 + \left(\frac{\beta}{2} - \epsilon\right) H_2O + \epsilon H_2S + \frac{\delta}{2} N_2 + \text{ash} \quad (17)$$

Kinetic Equation

$$\phi = (2Z + 2)/(Z + 2) \text{ for } d_p \leq 0.005 \text{ cm} \quad (18)$$

$$\phi = [(2Z + 2) - Z(d_p - 0.005)/0.095](Z + 2) \quad (19)$$

$$\text{for } 0.005 \text{ cm} < d_p \leq 0.1 \text{ cm}$$

$$\phi = 1.0 \text{ for } d_p > 0.1 \text{ cm} \quad (20)$$

$$Z = 2{,}500 \exp(-6{,}249/T) \quad (21)$$

$$T = (T_c + T_g)/2 \text{ in K}$$

$$K_s = 8{,}710 \exp(-17{,}967/T_c) \quad (22)$$

$$K_{\text{diff}} = \frac{0.292D}{d_p T} \quad (23)$$

$$D = 4.26 \left(\frac{T_g}{1{,}800}\right)^{1.75} \left(\frac{1}{P_t}\right) \quad (24)$$

Char-Steam Reaction

$$C_\alpha H_\beta O_\gamma N_\delta S_\epsilon A + (\alpha - \gamma)H_2O \rightarrow \alpha CO + (\alpha - \gamma + \frac{\beta}{2} - \epsilon)H_2 + \epsilon H_2S + \frac{\delta}{2} N_2 + \text{ash} \quad (25)$$

Kinetic Equation

$$K_s = 247 \cdot \exp(-21{,}060)/T_c) \quad (26)$$

$$K_{\text{diff}} = 10 \times 10^{-4} \left(\frac{T}{2{,}000}\right)^{0.75} / (p_t d_p) \quad (27)$$

$$K_{\text{eq}} = \exp[17.644 - 30{,}260/(1.8T_c)] \quad (28)$$

$$P_1 - P_1^* = P_{H_2O} - \frac{P_{H_2} - P_{CO}}{K_{\text{eq}}} \quad (29)$$

Char-Carbon Dioxide Reaction

$$C_\alpha H_\beta O_\gamma N_\delta S_\epsilon A + \alpha CO_2 \rightarrow 2\alpha CO + \frac{\gamma}{2} H_2O + \left(\frac{\beta}{2} - \epsilon - \gamma\right) H_2 + \epsilon H_2S + \frac{\delta}{2} N_2 + \text{ash} \quad (30)$$

Kinetic Equation

$$K_S = 247 \exp(-21{,}060/T_c) \quad (31)$$

$$K_{\text{diff}} = 7.45 \times 10^{-4} \left(\frac{T}{2{,}000}\right)^{0.75} / (p_t d_p) \quad (32)$$

$$P_1 - P_1^* = P_{CO_2} \quad (33)$$

Char-Hydrogen Reaction

$$C_\alpha H_\beta O_\gamma N_\delta S_\epsilon A + \left(2\alpha + \gamma + \epsilon - \frac{\beta}{2}\right) H_2 \rightarrow \alpha CH_4 + \gamma H_2O + \epsilon H_2S + \frac{\delta}{2} N_2 + \text{ash} \quad (34)$$

Kinetic Reaction

$$K_S = 0.12 \exp(-17{,}921)/T_C) \quad (35)$$

$$K_{\text{diff}} = 1.33 \times 10^{-3} \left(\frac{T}{2{,}000}\right)^{0.75} / (d_p p_t) \quad (36)$$

$$K_{\text{eq}} = \frac{0.175}{34{,}713} \exp[18{,}400/(1.8T_c)] \quad (37)$$

$$P_1 - P_1^* = P_{H_2} - \sqrt{P_{CH_4}/K_{\text{eq}}} \quad (38)$$

The gas-phase reactions occurring in the gasification section have been investigated by Singh and Saraf (1977), Wen and Chaung (1979), and Zahradnik and Grace (1974).

Water-Gas Shift Reaction

$$CO + H_2O \rightleftharpoons CO_2 + H_2 \quad (39)$$

Kinetic Equation

$$\text{Rate} = F_w \cdot (2.877 \times 10^5) \cdot \frac{1}{P_t} \times \left(P_{CO} - \frac{P_{CO_2} \cdot P_{H_2}}{K_{\text{eq}} \cdot P_{H_2O}} \cdot \exp\left(-\frac{27{,}760}{1.987T}\right)\right) \times p_f \cdot R_a(T) \frac{\text{gmol}}{\text{(s)(g of ash)}} \quad (40)$$

$$p_f = P_t\ (0.5 - P_{t/250}) \quad (41)$$

$$R_a(T) = \exp\left(-8.91 + \frac{5{,}553}{T}\right) \quad (42)$$

$$F_w = 0.2 \quad (43)$$

Methane-Steam Reaction

$$CH_4 + H_2O \rightleftharpoons CO + 3H_2 \quad (44)$$

Kinetic Equation

$$\frac{dC_{CH_4}}{dt} = -KC_{CH_4} \quad (45)$$

$$K = 312 \exp(-30{,}000/RT) \text{ in s}^{-1} \quad (46)$$

The net rate of char consumption due to the char-oxygen, char-steam, char-carbon dioxide, char-hydrogen reactions per unit volume of the solids in the reactor, designated as Γ (g/cm^3·s) in the reactor modeling equations discussed in the following section can be written as

$$\Gamma = \begin{cases} \frac{3}{R_p}[r_1 + r_2 + r_3] \text{ for combustion reaction} \\ \frac{3}{R_p}[r_2 + r_3 + r_4] \text{ for gasification section} \end{cases} \quad (47)$$

Model Development

A steady-state one-dimensional model for the reactor system has been formulated. The basic assumptions have been:

(1) The solid-gas phases are assumed to be completely mixed. A compartment-in-series approach is employed. Each compartment is treated as a stirred-tank reactor. The nature of mixing between the solid and gas phases can have a significant effect on the final carbon conversion and product composition.

(2) Radial dispersion is neglected.

(3) Due to a very dilute system, interactions among particles are neglected. Ash layer is assumed to remain on particle surface, hence, unreacted core shrinking model is assumed.

(4) Ideal gas equation of state is assumed to hold.

(5) The temperature of solid is uniform throughout the particle (i.e., the temperature gradients within the particle are negligible).

(6) Ash is assumed as inert and it remains with the particle. The effect of ash as a catalyst has been formally neglected although this may have been accounted for indirectly when the kinetic equations were developed. Since the validity of the results depends on the kinetic equations, the final results will change if ash catalyzes the combustion reactions.

(7) The frictional force between the phases and the wall is neglected.

(8) No particle attrition is considered.

(9) Due to the high temperatures in the reactor, potential and kinetic energies have been neglected in comparison with thermal energy.

The compartment-in-series approach is tantamount to assuming plug flow for the solid and gas phases (Wen and Fan, 1975). The selection of 1 cm height compartments for a 3.3 m long reactor results in a dispersion number $(D/U_c l)$ equal to 0.0015 which is essentially plug flow.

The mass, momentum and energy balances for each compartment have been investigated by Arastroopour and Gidaspow (1979), Rowe and Henwood (1961), and Wen (1979).

Solid-Phase Mass Balance

$$(\epsilon\rho_c U_c)_{x+\Delta x} - (\epsilon\rho_c U_c)_x = -\Gamma\epsilon \tag{48}$$

Gas-Phase Mass Balance

$$((1-\epsilon)\rho_g U_g)_{x+\Delta x} - ((1-\epsilon)\rho_g U_g)_x = \Gamma\epsilon \tag{49}$$

Solid-Phase Momentum Balance

$$(\epsilon\rho_c U_c^2)_{x+\Delta x} - (\epsilon\rho_c U_c^2)_x + (\epsilon P_t)_{x+\Delta x} g_c - (\epsilon P_t)_x g_c = \epsilon\rho_c g - f_s\epsilon \tag{50}$$

Gas-Phase Momentum Balance

$$((1-\epsilon)\rho_g U_g^2)_{x+\Delta x} - ((1-\epsilon)\rho_g U_g^2)_x + ((1-\epsilon)P_t)_{x+\Delta x} g_c - ((1-\epsilon)P_t)_x g_c = (1-\epsilon)\rho_g g + f_s\epsilon \tag{51}$$

Drag Force per unit Volume of Particles (Arastroopour and Gidaspow, 1979)

$$f_s = \frac{3C_D\rho_g(1-\epsilon)^{-2.65}(U_g - U_c)^2}{4d_p} \tag{52}$$

Drag Coefficient (Rowe and Henwood, 1961)

$$C_D = \frac{24}{Re}(1 + 0.15Re^{0.687}) \text{ for } Re < 1{,}000$$

$$= 0.44 \text{ for } Re \geq 1{,}000 \tag{53}$$

Reynolds Number

$$Re = \frac{(1-\epsilon)\rho_g d_p |U_g - U_c|}{\mu_g} \tag{54}$$

Solid-Phase Thermal Balance

$$A_t[\epsilon\rho_c U_c C_{p_c} T_c)_{x+\Delta x} - (\epsilon\rho_c U_c C_{p_c} T_c)_x] = \frac{3\epsilon}{R_p} A_t \Delta x \left[eF\sigma(T_g^4 - T_c^4) + h_c(T_g - T_c) + \sum_j (-\Delta H_j) r_j\right] - H_{\text{loss},s-w} \cdot \Delta x \tag{55}$$

Gas-Phase Thermal Balance

$$A_t[((1-\epsilon)\rho_g U_g C_{p_g} T_g)_{x+\Delta x} - ((1-\epsilon)\rho_g U_g C_{p_g} T_g)_x] = -\frac{3\epsilon}{R_p} A_t \Delta x.\ [eF\sigma(T_g^4 - T_c^4) + h_c(T_g - T_c)] + \sum_k (-\Delta H_k) r_k A_t \Delta x - H_{\text{loss},g-w}\Delta x \tag{56}$$

TABLE 3. REACTIONS

Solid Phase:

j = reaction

1 = pyrolysis

2 = char-oxygen reaction

3 = char-steam reaction

4 = char-carbon dioxide reaction

5 = char-hydrogen reaction

6 = water-gas shift reaction (catalyzed by the mineral materials in char)

7 = methane-steam reforming reaction (catalyzed by the mineral materials in char)

Gas Phase:

k = reaction

1 = $H_2 + \frac{1}{2}O_2 \rightarrow H_2O$

2 = $CO + \frac{1}{2}O_2 \rightarrow CO_2$

3 = $CH_4 + 2O_2 \rightarrow CO_2 + 2H_2O$

4 = $C_6H_6 + 15/2\ O_2 \rightarrow 6CO_2 + 3H_2O$

5 = $CO + H_2O \rightleftharpoons CO_2 + H_2$

6 = $CH_4 + H_2O \rightleftharpoons CO + 3H_2$

Three Reaction Sections

Reaction Section	j	k
pyrolysis and volatile combustion	1	1, 2, 3, 4
combustion and gasification	2, 3, 4	1, 2, 3
gasification	3, 4, 5, 6, 7	5, 6

Convection and Conduction Heat Transfer Coefficient (Wen, 1979)

$$h_c = \frac{2K_g}{d_p} \tag{57}$$

Reactions occurring in the solid and gas phases for each reaction section have been summarized in Table 3.

An approximate approach followed by Wen (1979) has been followed to compute heat exchange between the gas and the reactor wall.

(1) In the combustion zones, 30% of the total heat generated by reactions is transferred from gas phase to the reactor wall, which is about 7–10% of the heating value of the raw fuel.

(2) The rate of heat exchange per unit area of reactor wall, between the gas and the reactor wall, is calculated by $U_0(T_g - T_w)$, in the zones following combustion zones. The value of U_0 selected is temperature, a linear correlation of the wall temperature is assumed, which has been used by Wen (1979).

$$T_w = 2{,}100 - 600(x/L) \text{ in } °\text{F}. \tag{58}$$

Because of very dilute system, the viewing factor, F, for radiation heat transfer between gas and fuel particles can be assumed to be 1.0. The emissivity of the gas mixture is selected to be 0.9 for the Texaco entrained-bed gasifier.

SOLUTION PROCEDURE

The solid-phase thermal balance, Eq. 55, can be written as

$$\frac{dT_c}{dx} = \left\{\frac{3\epsilon}{R_p}\left[[eF\sigma(T_g^4 - T_c^4) + h_c(T_g - T_c)] + \sum_j (-\Delta H_j) r_j\right] - C_{p_c}\rho_{ci}U_{ci}T_{ci}\frac{d\epsilon}{dx} - C_{p_c}\rho_{ci}\epsilon_i T_{ci}\frac{dU_c}{dx} - C_{p_c}T_{ci}\epsilon_i U_{ci}\frac{d\rho_c}{ex}\right\} \{C_{p_c}\epsilon_i\rho_{ci}U_{ci}\}^{-1} \tag{59}$$

Combining the gas-phase and solid-phase thermal balances, the following overall heat balance is obtained.

$$((1-\epsilon)\rho_g U_g C_{p_g} T_g + \epsilon\rho_c U_c C_{p_c} T_c)_{x+\Delta x} - ((1-\epsilon)\rho_g U_g C_{p_g} T_g + \epsilon\rho_c U_c C_{p_c} T_c)_x = \frac{3\epsilon}{R_p}\sum_j (-\Delta H_j) r_j \Delta x + \sum_k (-\Delta H_k) r_k \Delta x - H_{\text{loss, gas}} \tag{60}$$

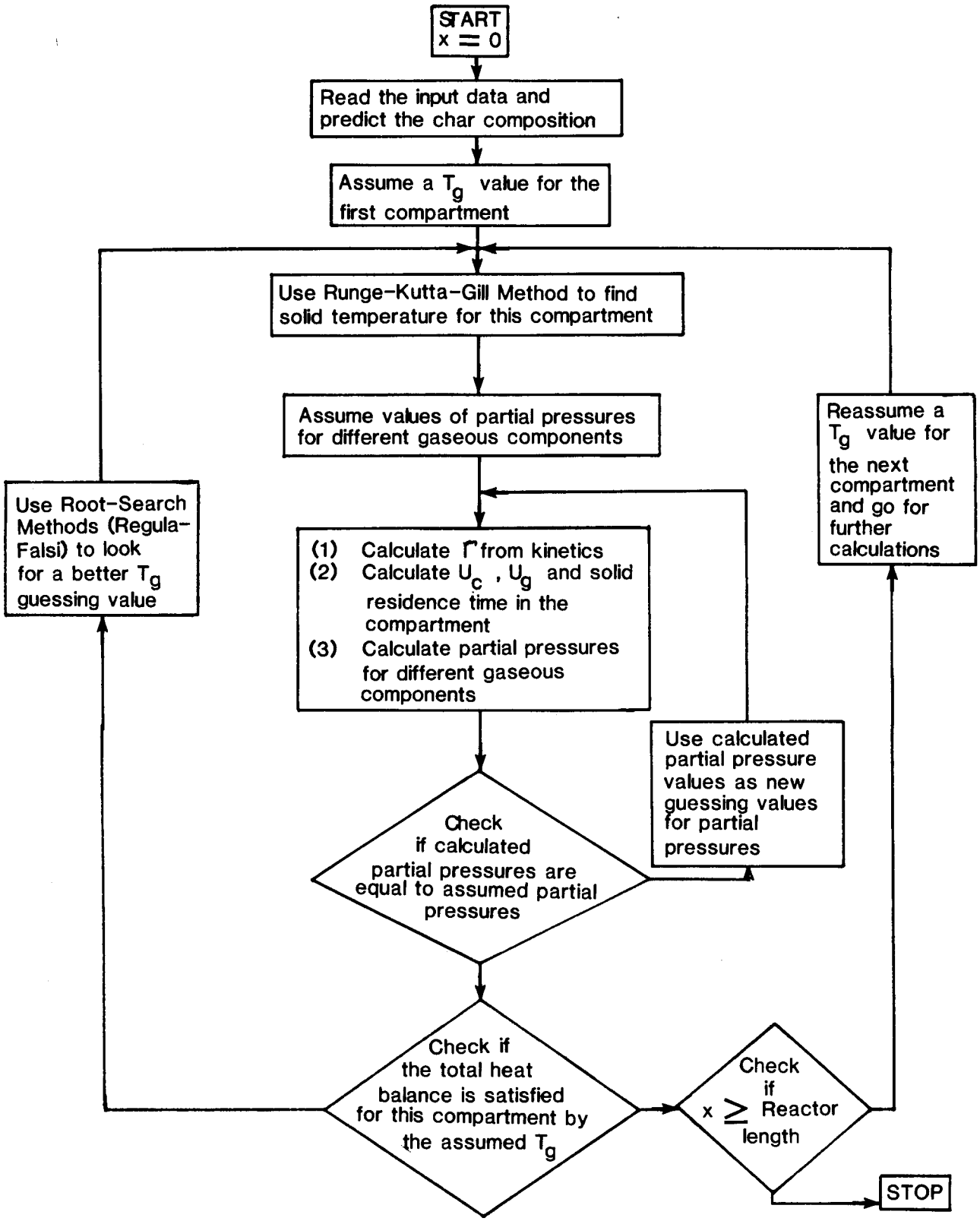

Figure 3. Computer flow diagram for solving the model equations.

Equations 58 and 59 are used to compute the solid and gas temperatures, respectively.

The mass and momentum balances for the solid and gas phases are solved simultaneously as follows:

$$X = A^{-1}C \tag{61}$$

where $X = (\Delta U_c, \Delta U_g, \delta p, \Delta\epsilon)$ and the elements of the A matrix and vector C

$$A_{11} = \epsilon_i \rho_{ci}$$

$$A_{12} = 0$$

$$A_{13} = 0$$

$$A_{14} = \rho_{ci} U_{ci} + \Gamma \Delta x$$

$$A_{21} = 0$$

TABLE 4. OPERATING CONDITIONS FOR SEVEN TYPICAL RUNS OF TEXACO'S PILOT-PLANT TESTS

Feedstock Source (Run Number)	Feed Rate: Fuel Rate (g/s)	Feed Rate: H_2O/Fuel	Feed Rate: O_2/Fuel	Feed Temperature (K): Fuel	Feed Temperature (K): Steam	Feed Temperature (K): Oxygen
H-coal residue from Illinois #6 coal (Run I-1)	76.66	0.241	0.866	505.22	696.67	298
H-coal residue from Illinois #6 (Run I-2)	81.18	0.314	0.7682	496.33	676.33	298
H-coal residue from Illinois #6 (Run W-1)	86.0	0.318	0.90	513.55	692.44	298
SRC II Vacuum Flash Drum Bottoms	126.11	0.30	0.70	505.22	696.67	298
Exxon DSP Vacuum Tower Bottoms	126.11	0.50	0.79	505.22	696.67	298
Western Coal used in coal-water slurry runs	186.78	0.52	0.91	400	400	600
Eastern coal used in coal-water slurry runs	133.5	0.79	0.87	400	400	600

$$A_{22} = (1 - \epsilon_i)\rho_{gi}$$

$$A_{23} = 0$$

$$A_{24} = -\rho_{gi}U_{gi} - \Gamma\Delta x$$

$$A_{31} = 2\epsilon_i\rho_{ci}U_{ci} + \left(\frac{\partial f_s}{\partial U_c}\right)_i \Delta x$$

$$A_{32} = \left(\frac{\partial f_s}{\partial U_g}\right)_i \Delta x$$

$$A_{33} = \epsilon_i \cdot g_c$$

$$A_{34} = \rho_{ci}U_{ci}^2 + P_{ti}g_c - \rho_{ci}g\Delta x + \left(\frac{\partial f_s}{\partial \epsilon}\right)_i \Delta x$$

$$A_{41} = -\left(\frac{\partial f_s}{\partial U_c}\right)_i \Delta x$$

$$A_{42} = -\left(\frac{\partial f_s}{\partial U_g}\right)_i \Delta x + 2(1 - \epsilon_i)\rho_{gi}U_{gi}$$

$$A_{43} = (1 - \epsilon_i)g_c$$

$$A_{44} = \rho_{gi}g\Delta x - P_{ti}g_c - \left(\frac{\partial f_s}{\partial \epsilon}\right)_i \Delta x - \rho_{gi}U_{gi}^2$$

$$C_1 = \epsilon_i U_{ci}\Delta\rho_c - \Gamma\epsilon_i\Delta x$$

$$C_2 = -U_{gi}(1 - \epsilon_i)\Delta\rho_g + \Gamma\epsilon_i\Delta x$$

$$C_3 = -\epsilon_i U_{ci}^2\Delta\rho_c + \epsilon_i\rho_{ci}g\Delta x + \epsilon_i g\Delta\rho_c\Delta_x - \left(\frac{\partial f_s}{\partial \rho_{gi}}\right)\Delta\rho_g\Delta x - f_{si}\Delta x$$

$$C_4 = (1 - \epsilon_i)\rho_{gi}g\Delta x + (1 - \epsilon_i)g\Delta\rho_g\Delta x + \left(\frac{\partial f_s}{\partial \rho_g}\right)_i \Delta\rho_g\Delta x + f_{si}\Delta_x - U_{gi}^2(1 - \epsilon_i)\Delta\rho_g$$

i = inlet conditions

The partial pressures of gaseous components leaving the compartment are calculated using the following material balance equations.

$$\alpha_1 = \frac{\text{total mol of gaseous components leaving compartments}}{\text{total mol of gaseous components entering compartments}}$$

$$\alpha_1 = \frac{F_{\text{out}}^g}{F_{\text{in}}^g} \tag{62}$$

For a stirred-tank reactor

$$-\frac{V'\epsilon}{F_{\text{in}}^g} = \frac{p_{\text{in}}^1 - \alpha_1 p_{\text{out}}^1}{P_t \sum_{p=1}^{m} r_p^1} \tag{63}$$

$$\sum_{1=1}^{n} p_{\text{out}}^1 = P_t \tag{64}$$

The partial pressures of the gaseous species leaving the compartment are computed using Eqs. 62, 63 and 64.

The solution procedure shown in Figure 3 is as follows:

(1) Assume a value for the gas-phase temperature (T_g) in the compartment.

(2) Calculate solid-phase temperature, T_c, from Eq. 59, using Runge-Kutta-Gill method.

(3) Assume the values of partial pressures for gaseous components leaving the compartment.

(4) Calculate value of Γ from Eq. 47. Calculate values of U_c, U_g and solid residence time in the compartment from Eq. 61. Calculate partial pressures for gaseous components leaving the compartment from Eqs. 62, 63 and 64. If the partial pressures meet the required error criteria, check total heat balance. Otherwise, use calculated partial pressure values as new guessing values and repeat the procedure again.

(5) Check total heat balance using Eq. 60. If the total heat balance satisfies the required error criteria, repeat the procedure for the next compartment. Othersise, use root-search method (Regula-Falsi) to find a better value of T_g and repeat the procedure again.

RESULTS AND DISCUSSIONS

The Texaco reactor was simulated for 27 runs using coal liquefaction residues and two runs using coal-water slurries as feedstock. Table 4 shows the operating conditions. Parameter values for these seven typical runs are as follows.

Gasifier

Pressure: Coal liquefaction residue runs 24.32×10^5 N/m^2 (24 atm)

Coal water slurry runs 21.28×10^5 N/m^2

Diameter: 152.4 cm (5 ft)

Height: 330 cm (combustion section)

Solid Phase

Initial density of coal liquefaction residue = 1.18 cm/cm^3

Initial solid velocity = 50 cm/s (assumed)

Initial particle size = Wyodak coal liquefaction residue, 400μm

All other runs, 350μm

Specific heat = 0.45 cal/g·°C

Gas Phase

Specific heats for gases and heats of combustion (*Perry's Handbook*)

Emissivity of gas = 0.9

Overall heat transfer coefficient between gas and reactor wall = 122 kcal/hr·m^2·°C (25 Btu/h·ft^2·°F)

The results of the model predictions have been summarized in Table 5 along with the reported experimental results (Robin, 1964).

The gas composition leaving the gasifier and the final carbon conversion depend on three essential operating parameters: the fuel rate, the oxygen to fuel ratio and the steam-fuel ratio. In our study, due to lack of inlet velocity data, the inlet velocity of solids was assumed to be 50 cm/s for all the runs. This lack of experimental data makes it difficult to exactly compare the numerical results of the simulation program with experimental data.

Significant deviations in the gas composition and carbon conversions were found for runs where the fuel rate is higher. This can be attributed to the error in the inlet velocity of the solids which in the experimental run was probably much higher than 50 cm/s

TABLE 5. COMPUTATIONAL RESULTS: THE MODEL VS. TEXACO ENTRAINED-BED PILOT-PLANT GASIFIER

RUN NO.	INPUT CONDITION			Source	CO	H_2	CO_2	CH_4	H_2S	N_2	Carbon Conversion %
	Fuel Rate (g/sec)	$\frac{O_2}{Fuel}$	$\frac{Steam}{Fuel}$		Flow Rate g/sec (Vol %)	Flow Rate g/sec (Vol %)	Flow Rate g/sec (Vol %)	Flow Rate g/sec (Vol %)	Flow Rate g/sec (Vol %)	Flow Rate g/sec (Vol %)	
I-1	76.66	0.866	0.241	Exp	123.77 (57.57)	6.01 (39.13)	9.985 (2.95)	0.15 (0.12)	0.133 (0.06)	0.53 (0.12)	98.64
				Model	120.8 (55.46)	6.22 (39.99)	13.51 (3.95)	0.135 (0.109)	0.720 (0.272)	0.476 (0.219)	98.101
I-2	81.18	0.768	0.318	Exp	112.52 (53.06)	6.211 (41.00)	17.2 (5.15)	0.56 (0.46)	0.59 (0.21)	0.1513 (0.07)	90.66
				Model	102.03 (51.794)	6.26 (41.688)	19.65 (5.95)	0.18 (0.15)	0.547 (0.214)	0.461 (0.219)	88.26
I-3	82.202	0.813	0.309	Exp	121.5 (54.56)	6.24 (39.31)	19.26 (5.51)	0.114 (0.08)	0.67 (0.26)	0.133 (0.11)	98.28
				Model	121.35 (54.29)	6.35 (39.8)	18.59 (5.29)	0.119 (0.094)	0.759 (0.280)	0.531 (0.238)	97.84
I-4A	79.456	0.807	0.323	Exp	116.0 (55.70)	5.78 (38.90)	16.74 (5.11)	0.15 (0.12)	0.32 (0.11)	0.0124 (0.00)	97.24
				Model	112.99 (53.071)	5.99 (39.43)	23.45 (7.01)	0.086 (0.07)	0.518 (0.2)	0.46 (0.216)	98.11
I-4B	81.846	0.797	0.310	Exp	119.54 (54.90)	6.107 (39.26)	18.14 (5.30)	0.185 (0.14)	0.70 (0.23)	0.24 (0.11)	97.34
				Model	118.1 (53.82)	6.26 (39.94)	19.77 (5.733)	0.112 (0.09)	0.526 (0.198)	0.47 (0.214)	97.047
I-5A	71.64	0.8263	0.352	Exp	103.32 (54.02)	5.30 (38.78)	19.972 (6.64)	0.0852 (0.07)	0.57 (0.21)	0.428 (0.22)	98.875
				Model	95.81 (51.63)	4.94 (37.288)	30.63 (10.5)	10.05 (0.047)	0.670 (0.298)	0.44 (0.24)	98.169
I-5B	65.0	0.817	0.392	Exp	92.3 (52.48)	5.007 (39.85)	19.987 (7.22)	0.086 (0.08)	0.73 (0.31)	0.0034 (0.00)	98.868
				Model	91.65 (51.96)	5.06 (40.18)	20.15 (7.27)	0.06 (0.061)	0.615 (0.287)	0.417 (0.237)	98.26
I-5C	56.264	0.832	0.429	Exp	81.853 (51.39)	4.53 (39.83)	20.61 (8.23)	0.0434 (0.04)	0.8035 (0.41)	0.0734 (0.04)	98.885
				Model	76.68 (50.949)	4.26 (39.601)	20.98 (8.87)	0.0414 (0.048)	0.534 (0.292)	0.359 (0.239)	97.92
I-6	87.73	0.774	0.291	Exp	125.2 (55.03)	6.41 (39.43)	17.95 (5.01)	0.27 (0.20)	0.3 (0.1)	0.351 (0.17)	97.22
				Model	119.03 (53.46)	6.31 (39.67)	21.69 (6.2)	0.118 (0.0933)	0.866 (0.321)	0.553 (0.249)	93.84
I-7A	90.974	0.7757	0.282	Exp	130.3 (55.33)	6.67 (39.62)	17.1 (4.62)	0.27 (0.20)	0.292 (0.08)	0.213 (0.009)	96.826
				Model	122.16 (53.26)	6.51 (39.75)	22.95 (6.37)	0.119 (0.091)	0.767 (0.275)	0.569 (0.248)	93.64
I-7B	95.392	0.782	0.267	Exp	139.75 (55.87)	6.975 (39.03)	17.3 (4.40)	0.197 (0.13)	0.866 (0.26)	0.640 (0.25)	96.992
				Model	127.47 (53.64)	6.66 (39.23)	24.32 (6.512)	0.128 (0.095)	0.791 (0.274)	0.597 (0.252)	91.97
I-8A	92.13	0.797	0.247	Exp	140.7 (57.38)	6.732 (38.43)	14.27 (3.70)	0.13 (0.09)	0.91 (0.30)	0.102 (0.04)	98.641
				Model	128.88 (55.1)	6.48 (38.792)	20.13 (5.48)	0.136 (0.102)	0.77 (0.271)	0.58 (0.249)	93.36
I-8B	95.07	0.8016	0.239	Exp	145.8 (57.67)	6.913 (38.28)	14.4 (3.62)	0.058 (0.03)	0.80 (0.25)	0.204 (0.08)	98.663
				Model	130.01 (54.56)	6.43 (37.8)	26.3 (7.025)	0.117 (0.087)	0.798 (0.276)	0.595 (0.250)	93.56
I-8C	92.86	0.800	0.246	Exp	141.073 (57.02)	6.785 (38.39)	15.28 (3.93)	0.071 (0.04)	1.18 (0.37)	0.46 (0.18)	98.605
				Model	129.71 (55.09)	6.49 (38.605)	21.01 (5.68)	0.133 (0.099)	0.781 (0.273)	0.585 (0.249)	93.7
I-9	87.79	0.787	0.268	Exp	125.4 (57.49)	5.966 (38.29)	12.89 (3.76)	0.096 (0.07)	0.80 (0.26)	0.148 (0.06)	97.45
				Model	123.86 (54.87)	6.33 (39.237)	18.86 (5.31)	0.129 (0.10)	0.632 (0.231)	0.559 (0.248)	94.62
I-10	129.77	0.8346	0.276	Exp	201.16 (55.18)	10.22 (39.24)	26.92 (4.69)	0.15 (0.26)	0.58 (0.10)	1.73 (0.47)	99.158
				Model	155.13 (50.24)	8.6 (38.97)	49.89 (10.28)	0.135 (0.077)	0.852 (0.227)	0.628 (0.204)	84.674

TABLE 5. *Continued*

RUN NO.	INPUT CONDITION			Source	CO	H_2	CO_2	CH_4	H_2S	N_2	Carbon Conversion %
	Fuel Rate (9/sec)	$\frac{O_2}{Fuel}$	$\frac{Steam}{Fuel}$		Flow Rate 9/sec (vol %)	Flow Rate 9/sec (vol %)	Flow Rate 9/sec (vol %)	Flow Rate 9/sec (vol %)	Flow Rate 9/sec (vol %)	Flow Rate 9/sec (vol %)	
I-11	132.79	0.8484	0.279	Exp	204.16 (54.79)	10.57 (39.72)	29.96 (5.11)	0.193 (0.09)	0.68 (0.12)	0.42 (0.11)	99.187
				Model	155.25 (49.37)	8.87 (39.5)	52.43 (10.61)	0.1375 (0.077)	0.880 (0.231)	0.654 (0.208)	83.78
W-1	86.0	0.90	0.318	Exp	143.2 (56.96)	6.8325 (38.04)	19.15 (4.84)	0.0517 (0.03)	0.00 (0.00)	0.19 (0.07)	98.98
				Model	139.29 (55.08)	7.00 (38.81)	22.83 (5.75)	0.122 (0.085)	0.031 (0.01)	0.656 (0.26)	98.157
W-2	87.231	0.859	0.286	Exp	146.25 (57.67)	6.865 (37.90)	17.1 (4.29)	0.0898 (0.06)	0.0325 (0.00)	0.078 (0.03)	99.17
				Model	143.83 (57.475)	6.73 (37.663)	17.69 (4.49)	0.147 (0.103)	0.0275 (0.009)	0.629 (0.251)	97.86
W-3A	128.49	0.844	0.253	Exp	212.71 (57.80)	9.85 (37.47)	25.66 (4.43)	0.22 (0.10)	0.00 (0.00)	0.553 (0.15)	99.393
				Model	174.68 (54.43)	8.38 (36.56)	43.44 (8.613)	0.162 (0.088)	0.0814 (0.021)	0.926 (0.288)	87.678)
W-3B	128.67	0.86	0.264	Exp	208.2 (56.02)	10.5 (37.02)	34.016 (5.82)	0.129 (0.06)	0.103 (0.01)	0.68 (0.18)	99.395
				Model	177.83 (54.44)	8.63 (36.963)	42.08 (8.198)	0.172 (0.092)	0.083 (0.021)	0.942 (0.288)	88.473
W-4	125.66	0.857	0.273	Exp	211.44 (57.61)	10.06 (37.77)	23.77 (4.12)	0.28 (0.13)	0.00 (0.00)	1.20 (0.32)	98.765
				Model	167.09 (52.744)	8.24 (36.404)	52.29 (10.5)	0.133 (0.074)	0.079 (0.021)	0.806 (0.255)	87.34
W-5	129.826	0.854	0.263	Exp	215.34 (57.00)	10.343 (38.32)	25.45 (4.28)	0.34 (0.15)	0.032 (0.00)	0.734 (0.19)	98.211
				Model	167.95 (52.331)	8.71 (37.999)	46.89 (9.29)	0.16 (0.087)	0.055 (0.014)	0.865 (0.27)	83.90
W-6	132.82	0.855	0.318	Exp	215.07 (54.91)	10.97 (39.20)	33.84 (5.49)	0.41 (0.18)	0.00 (0.00)	0.706 (0.18)	97.900
				Model	163.12 (49.626)	8.99 (38.333)	60.44 (11.70)	0.133 (0.071)	0.038 (0.009)	0.854 (0.260)	83.374
W-7	135.64	0.94	0.310	Exp	220.02 (54.24)	11.00 (37.98)	48.576 (7.62)	0.00 (0.00)	0.00 (0.00)	0.477 (0.11)	99.676
				Model	189.54 (52.39)	9.59 (37.1)	57.84 (10.175)	0.159 (0.0777)	0.0067 (0.002)	0.901 (0.249)	89.89

B. Using SRC II Vacuum Flash Drum Bottoms as feedstock:

INPUT CONDITION			Source	CO	H_2	CO_2	H_2O	CH_4	H_2S	N_2	Carbon Conversion %
Fuel Rate (9/sec)	$\frac{O_2}{Fuel}$	$\frac{Steam}{Fuel}$		FlowRate 9/sec (vol %)	FlowRate 9/sec (vol %)	FlowRate 9/sec (vol %)	FlowRate 9/sec (vol %)	FlowRate 9/sec (vol %)	FlowRate 9/sec (vol %)	FlowRate 9/sec (vol %)	
126.11	0.77	0.30	Exp	167.58 (53.51)	6.936 (3.10)	32.98 (6.7)	14.50 (7.2)	0.00 (0.00)	4.1 (1.04)	1.566 (0.5)	99
			Model	157.26 (50.62)	7.04 (31.75)	41.91 (8.58)	16.04 (8.04)	0.109 (0.06)	1.95 (0.52)	1.27 (0.40)	96.41

C. Using Exxon DSP Vacuum Tower Bottoms as feedstock:

126.11	0.79	0.5	Exp	176.98 (45.6)	9.37 (33.8)	45.87 (7.52)	29.69 (11.9)	0.00 (.0.00)	3.81 (0.78)	1.475 (0.38)	99
			Model	135.51 (37.16)	8.4 (32.29)	74.03 (12.91)	39.54 (16.88)	0.087 (0.038)	1.69 (0.37)	1.10 (0.304)	87.8

TABLE 5. *Continued*

D. Coal-Water Slurry Runs:

COAL TYPE	INPUT CONDITION			Source	CO	H_2	CO_2	CH_4	H_2S	N_2	Carbon Conversion %
	Coal Rate (9/sec)	$\frac{O_2}{Coal}$	$\frac{Water}{Coal}$		Vol. %	Vol. %	Vol. %	Vol. %	Vol. %	Vol. %	
Western	186.78	0.91	0.51	Exp	50.71	35.79	13.14	0.09	0.03	0.24	92.7
				Model	42.46	37.093	20.05	0.028	0.075	0.295	92.79
Eastern	133.5	0.87	0.79	Exp	41.55	36.15	20.64	0.40	0.85	0.38	85.8
				Model	39.44	32.62	21.00	0.021	0.498	0.427	86.33

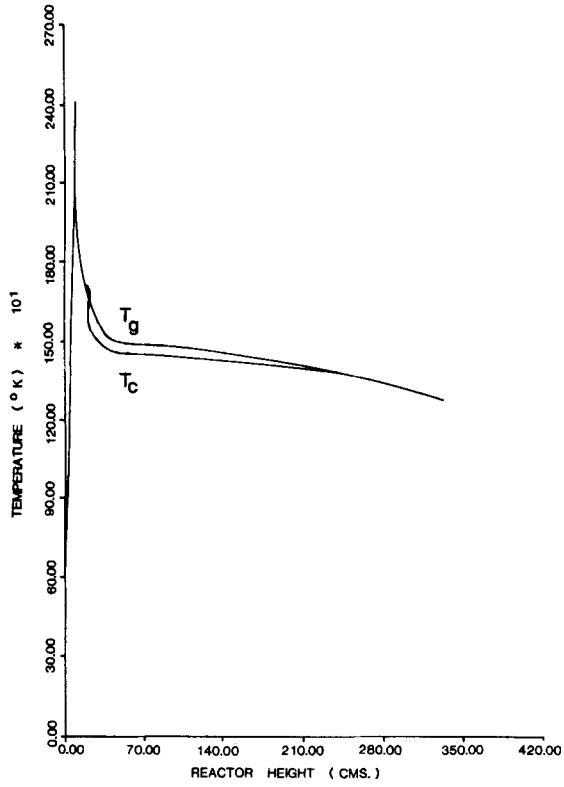

Figure 4. Temperature profiles for I-1 run.

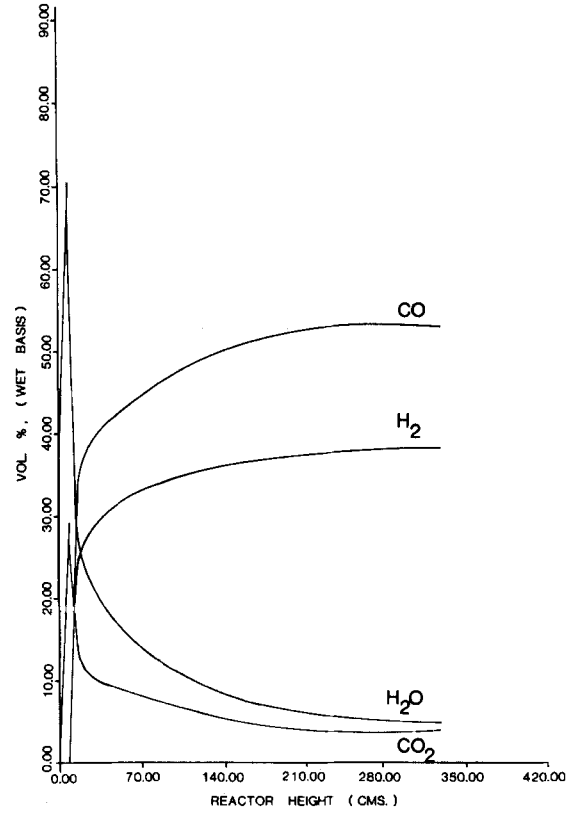

Figure 5. Product gas composition profiles for I-1 run.

assumed in the simulation program. At higher fuel (coal liquefaction residues) rates the particle (droplet) size becomes smaller, since the fuel is sprayed into the reactor through nozzles. Large particles (droplets) have greater terminal velocities and thus travel at higher velocities resulting in shorter residence time than smaller particles. On the other hand, the specific contact area between reacting gases and the fuel particle (droplet) is inversely proportional to the particle size. These two effects combine to give higher conversion for smaller (droplets) with higher inlet velocity.

The temperature, concentration and velocity profiles within the reactor have been shown in Figures 4 through 8 for Run No. I-1 using Illinois No. 6 coal. Figure 4 shows the solid and gas temperature profiles along the reactor height. Both the solid and gas temperatures undergo a rapid increase due to the highly exothermic combustion reactions attaining a maximum of 2,269 and 2,370 K respectively. At this point in the reactor the entire oxygen gets consumed and the endothermic reactions, namely, char-CO_2, char-steam, etc. become effective, reducing the and gas temperatures.

The change in gas composition over the reactor length have been shown in Figures 5 and 6. Steam and CO_2 concentration attain a maximum at a height when oxygen has just been consumed.

Figure 7 shows carbon conversion as a function of reactor height, indicating significant conversion in the first 100 cm of reactor height.

Figure 8 shows solid and gas velocities along the reactor height. Gas velocity increases as different gases are produced. Solid velocity increases initially and then decreases and attains a final value of 19.2 cm/s.

The solid velocity increases initially since the solid terminal velocity based on the inlet solid density is 101 cm/s which is higher then the inlet velocity of 50 cm/s. The maximum velocity is at-

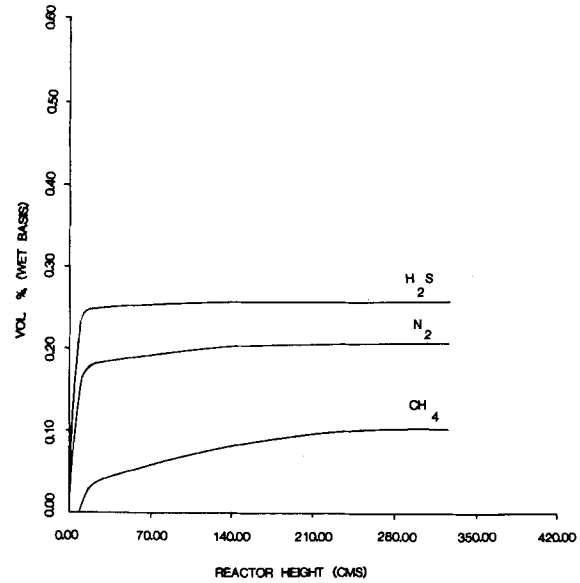

Figure 6. Product gas composition profiles for I-1 run.

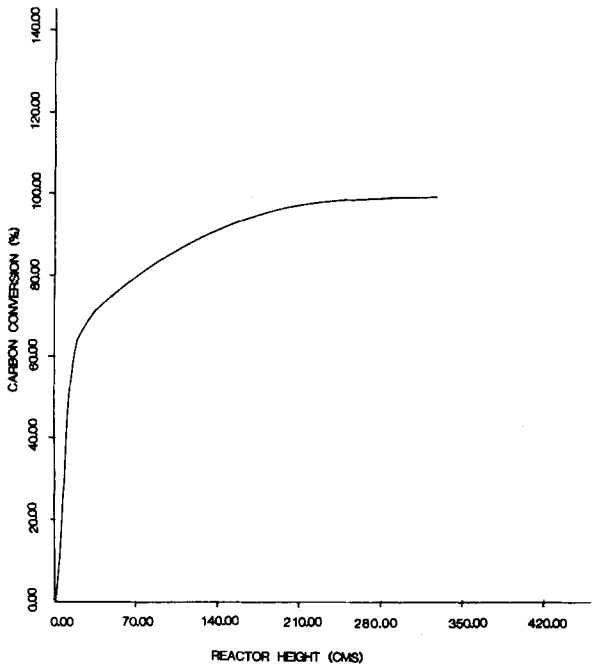

Figure 7. Carbon conversion profiles for I-1 run.

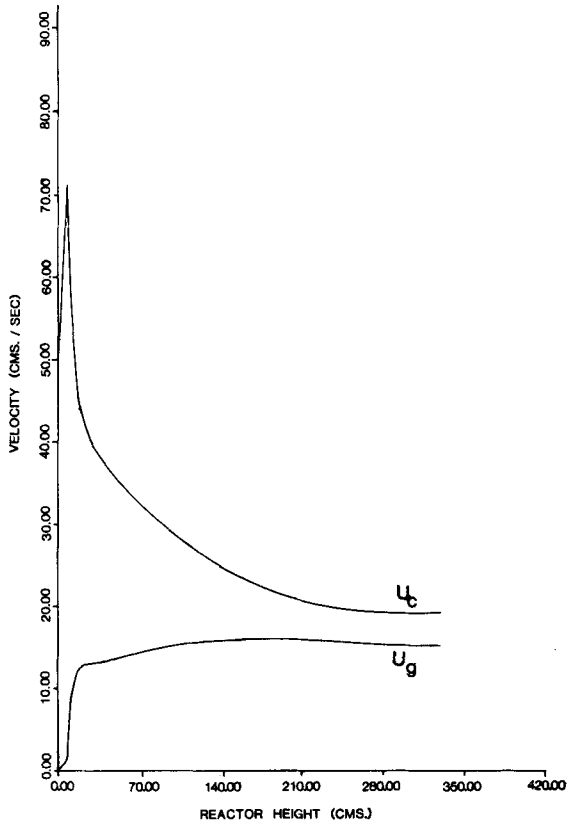

Figure 8. Velocity profiles for I-1 run.

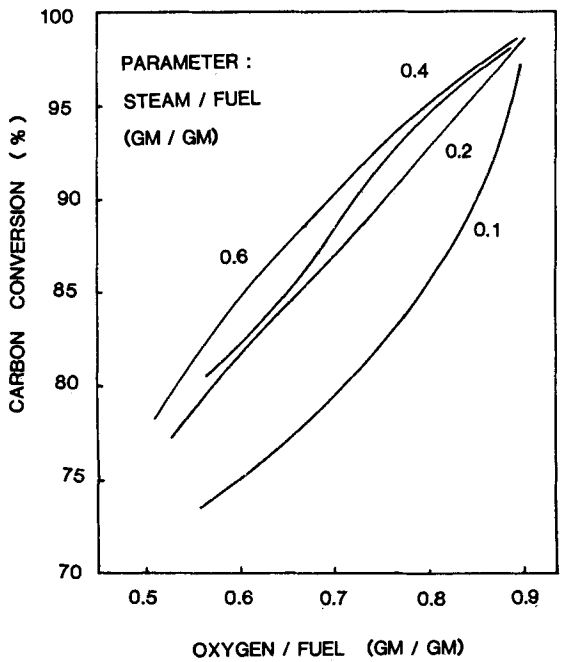

Figure 9. Effect of oxygen/fuel ratio on carbon conversion at various steam/fuel ratios.

tained at the exit of the pyrolysis section. The solid velocity decreases due to the decrease in solid density caused by the reaction. As the solid density decreases, the terminal velocity decreases and the solid particle follows this trend.

Parameter studies were made to understand the reactor performance for various operating conditions using the model. Figures 9 through 12 show the effect of oxygen-fuel and steam-fuel ratio on the final conversion and gas product distribution.

Figure 9 shows the effect of oxygen-fuel ratio on carbon conversion at various steam/fuel ratios feeding the coal residue from Illinois No. 6 coal into the Texaco pilot-plant gasifier. Figure 10 shows the effect of steam/fuel ratio on carbon conversion at various oxygen/fuel ratios using coal liquefaction residues as feedstock. It was found that oxygen/fuel ratio affects carbon conversion more than does the steam/fuel ratio. It was found that for this gasifier, the optimum (for maximum carbon conversion) oxygen/fuel ratio is between 0.8 and 0.9 to achieve 98–99% conversion. Depending on the oxygen/fuel ratio the optimal (for maximum carbon conversion) steam/fuel ratio ranges from about 0.3 to 0.6 for this gasifier using coal liquefaction residues as feedstock.

Figure 11 shows that oxygen/fuel ratio affects carbon conversion significantly but does not have a significant effect on the gas product distribution. On the contrary, steam/fuel ratio significantly

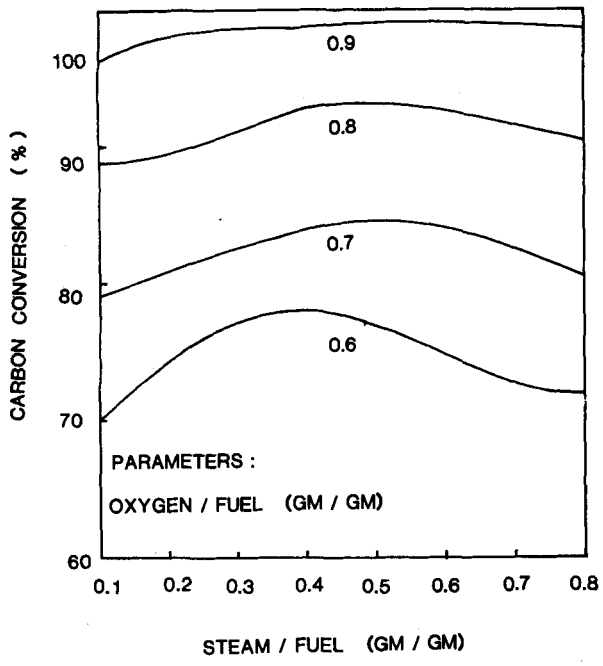

Figure 10. Effect of steam/fuel ratio on carbon conversion at various oxygen/fuel ratios.

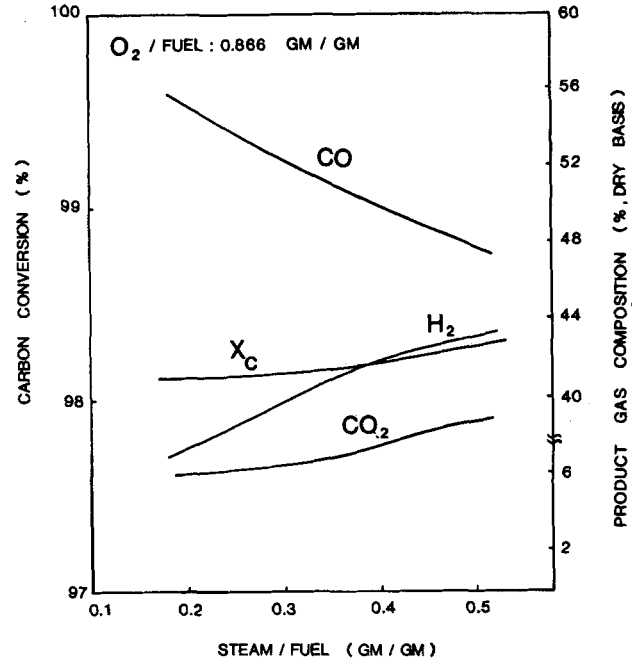

Figure 12. Effects of steam/fuel ratio on carbon conversion and major product gas composition at oxygen/fuel = 0.866 g/g.

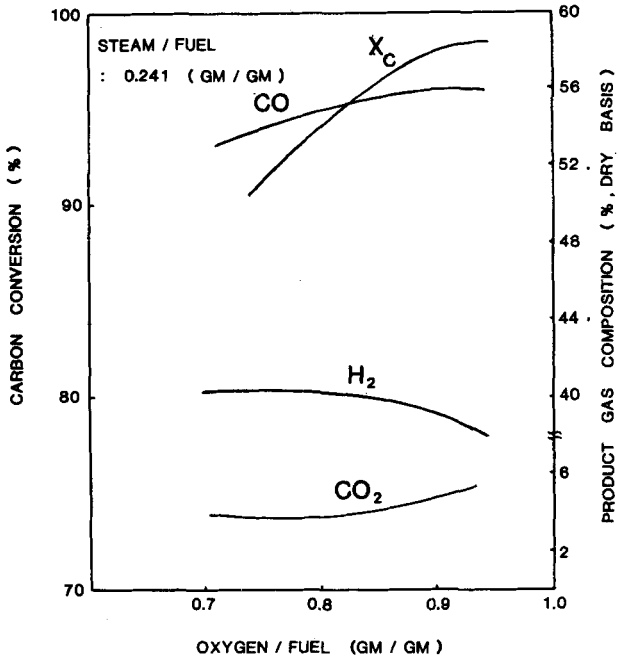

Figure 11. Effects of oxygen/fuel ratio on carbon conversion and major product gas composition at steam/fuel = 0.241 g/g.

affects the gas product distribution. Figure 12 shows the effect of steam/fuel ratio on conversion and gas product distribution at a fixed oxygen/fuel ratio. As the oxygen/fuel increases, the concentration of H_2 decreases but those of CO and CO_2 increases, keeping steam/fuel ratio, Figure 12, the concentration of H_2 and CO_2 increases but that of CO decreases. These concentration variations are due to the competition among char-oxygen, char CO_2, char-steam, and water-gas shift reactions.

A sensitivity analysis of the developed model was conducted with the char-gas reactions kinetic coefficients only, since the pyrolysis reaction rate does not significantly affect the final carbon conversion, as noted earlier. Qualitatively the analysis revealed that the char-oxygen kinetic coefficient had a major impact on the % carbon conversion. The char-steam kinetic coefficient also affected the % carbon conversion but not to the same degree as the char-oxygen kinetic coefficient.

Quantitatively, defining a char-gas reaction rate as

$$\text{rate} = K(P_1 - P_1^*) \tag{65}$$

where the coefficient K, according to Eq. 13, represents the effects of ash layer diffusion, gas film diffusion and chemical reactions. The sensitivity coefficient (S) is defined as follows:

$$S = \frac{\dfrac{\Delta\%C \text{ Conversion}}{\%C \text{ Conversion}}}{\dfrac{\Delta K}{K}} \tag{66}$$

The sensitivity coefficient depends on the type of runs and the operating conditions selected for the gasifier. For example, for I-1 run (H-coal residue from Illinois #6 coal) the sensitivity coefficient for the char-oxygen reaction was equal to 0.257 for an oxygen/fuel ratio of 0.86 and a steam fuel ratio of 0.24. The sensitivity coefficient for the same run for the char-steam reaction was 0.081.

ACKNOWLEDGMENT

I would like to thank Ms. Denterlein for patiently and accurately typing this paper.

NOTATION

A_t	= cross-sectional area of reactor (cm^2)
C_{pg}, C_{pc}	= specific heats of gas and solids respectively (cal/g·K)
C_D	= drag coefficient
C_n	= concentration in the nth compartment
d_p	= particle diameter (cm)
D	= diffusivity of gas (cm^2/s)
e	= emissivity of gas
f_s	= drag force on solids per unit volume of particles
F_w	= correction factor for water gas shift reaction
g	= gravity acceleration, (cm/s^2)

g_c = correction factor
h_c = convection heat transfer coefficient between gas and solid (cal/cm²·K·s)
$H_{loss,g\text{-}w}$ = heat exchange between gas and reactor wall (cal/cm·s)
ΔH_k = heat of reaction of kth reaction (cal/g)
ΔH_j = heat of reaction of jth reaction (cal/g)
K = overall kinetic constant defined by Eq. 65
K_s = surface reaction constant (g/cm²·atm·s)
K_{diff} = gas diffusion constant (g/cm²·atm·s)
K_{ash} = ash film diffusion constant (g/cm²·atm·s)
K_{eq} = equilibrium constant of water gas shift reaction
K_g = thermal conductivity of gas (cal/cm·K)
L = total effective reactor length (cm)
m = total number of reactions
n = total number of species
P_f = pressure correction factor
P_t = total pressure in reactor (atm)
$P_l - P_l^*$ = effective partial pressure of gas taking into account reverse reaction effect (atm)
p_{in}^l = partial pressure of lth gaseous component at the inlet of compartment
p_{out}^l = partial pressure of lth gaseous component at the exit of the compartment
R = gas constant
R_a = temperature correcting factor
R_p = outside radius of an unreacted-core-shrinking particle (cm)
r_c = radius of the unreacted core of an unreacted-core-shrinking particle (cm)
r_j = reaction rate of jth solid phase reaction (g/cm³·s)
r_k = reaction rate of kth gas involved reaction (g/cm³·s)
r_1 = rate of char-oxygen reaction
r_2 = rate of char-steam reaction
r_3 = rate of char-carbon dioxide reaction
r_4 = rate of char-hydrogen reaction
S = Sensitivity coefficient defined in Eq. 66
T_w = wall temperature (K)
T_g = gas-phase temperature (K)
T_c = solid-phase temperature (K)
T = $(T_c + T_g)/2$ (K)
U_g = gas-phase velocity (cm/s)
U_c = solid phase velocity (cm/s)
$\overline{U}_c$ = average solid velocity between compartments (cm/s)
V^* = total volatile content of coal (cm³/g)
V = volatile content at time t (cm³/g)
V^l = total volume of compartment
x = distance from the top of reactor (cm)
Δx = length of each compartment (cm)
y = ratio of r_c/R_p in an unreacted-core-shrinking particle, dimensionless

Greek Letters

ϵ = solid-phase volume fraction
ϵ_1 = voidage of ash layer
Φ = mechanism factor of combustion reaction
μ_g = gas viscosity (poise)
ρ_c, ρ_g = densities of solid and gas (g/cm³)
Γ = rate of char consumption, (g/cm³·s)
σ = Stefan-Boltzmann constant, (col/cm²·s·K⁴)

Subscripts

i = inlet conditions in compartment
j,k = reactions in solid and gas phase
l = gaseous component
m = total number of reactions
η = total number of gaseous species
α = stoichiometric coefficient for carbon
β = stoichiometric coefficient for hydrogen
γ = stoichiometric coefficient for oxygen
δ = stoichiometric coefficient for nitrogen
ϵ = stoichiometric coefficient for sulfur

Superscripts

g = gas phase
l = gaseous component
$*$ = equilibrium conditions

LITERATURE CITED

Anthony, D. B., and J. B. Howard, "Coal Devolatization and Hydrogasification," *AIChE J.*, **22**, 625 (1976).
Anthony, D. B., J. B. Howard, H. C. Hottel, and H. P. Meissner, "Rapid Devolatization of Pulverized Coal," *Fuel*, **55**, 121 (1976).
Arastoopour, H., and D. Gidaspow, "Vertical Pneumatic Conveying Using Four Hydrodynamic Models," *Ind. Eng. Chem. Fund.*, **18**, No. 2, 123 (1979).
Badzioch, S., and P. B. W. Hawksley, "Kinetics of Thermal Decomposition of Pulverized Coal Particles," *Ind. Eng. Chem. Process Dev.*, **9**, 521 (1970).
Bird, B. R., W. E. Stewart, and E. N. Lightfoot, *Transport Phenomena*, John Wiley & Sons, (1960).
Bissett, L. A., "An Engineering Assessment of Entrainment Gasification," MERC/RI—78/2, Morgantown Energy Research Center (April, 1978).
Black, T. R., "Alternative Energy Sources," Ed., T. Nejat Veziroglu, *Hydrocarbon Conversion Technology*, **7**, 2971, Hemisphere Publishing (1978).
Boothroyd, R. G., *Flowing Gas-Solids Suspensions*, Chapman and Hall Lts. (1971).
Carnahan, B., H. R. Luther, J. O. Wilkes, *Applied Numerical Analysis*, John Wiley & Sons (1969).
Dobner, S., "Modeling of Entrained Bed Gasification: The Issues," EPRI, Palo Alto, CA (Jan. 15, 1976).
Dutta, S., C. Y. Wen, and R. J. Belt, "Reactivity of Coal and Char, 1. In Carbon Dioxide Atmosphere," *Ind. Eng. Chem., Process Des, Dev.*, **16**, 20 (1977).
Field, M. A., D. W. Gill, B. B. Morgan and P. B. Hawksley, "Combustion of Pulverized Coal," BCURDA, Leatherhead (1967).
Field, M. A., "Rate of Combustion of Size-Graded Fractions of Char from a Low-Rate Coal Between 1200°K and 2000°K," *Combust. Flame*, **13**, 237 (1969).
Field, M. A., "Measurements of the Effect of Rank on Combustion Rates of Pulverized Coal," *Combust. Flame*, **14**, 237 (1970).
Goyal, A., "Mathematical Modeling of Entrained Flow Coal Gasification Reactors," Ph.D. Thesis, Illinois Inst. Technol., Chicago (1980).
Howard, J. B., and R. H. Essenhigh, "Pyrolysis of Coal Particles in Pulverized Fuel Flames," *Ind. Eng. Chem., Process Des. Dev.*, **6**, 74 (1967).
Jensen, G. A., "The Kinetics of Gasification of Carbon Contained in Coal Minerals at Atmospheric Pressure," *Ind. Eng. Chem., Process Des. Dev.*, **14**, 318 (1975).
Kane, R. S., and R. A. McCallister, "Scaling Laws and the Differential Equation of an Entrained Flow Coal Gasifier," *AIChE J.*, **24**, 55 (1978).
Klei, H. E., J. Sahagian, and D. W. Sundstrom, "Kinetics of the Activated Carbon-Stream Reaction," *Ind. Eng. Chem., Process Des. Dev.*, **14**, 470 (1975).
Levenspiel, O., *Chemical Reaction Engineering*, Wiley Eastern Ltd. (1972).
Loison, R., and R. Chauvin, "Pyrolyse Rapide Du Charbon," *Chim. Ind.*, **91**, 269 (1964).
Lowry, H. H., Ed., *Chemistry of Coal Utilization*, John Wiley & Sons (1980).
Perry, H. R., and C. H. Chilton, *Chemical Engineers' Handbook*, McGraw-Hill Ltd., Fifth Ed.
Robin, A. M., "Hydrogen Production from Coal Liquefaction Residues," EPRI Rtp., EPRI-AF-233 (Dec., 1976).
Robin, A. M., "Gasification of Residual Materials from Coal Liquefaction," L.O.E. Quarterly Report, FE-2247-11 (Oct., 1977).
Rowe, P. N., and G. A. Henwood, "Drag Forces in Hydraulic Model of Fluidized Bed," *Trans. Chem. Eng.*, **39**, 43 (1961).

Singh, C. P. P., and D. N. Saraf, "Simulation of High-Temperature Water-Gas Shift Reactors," *Ind. Eng. Chem., Process Des. Dev.*, **16**, No. 3, 313 (1977).
Smoot, L. D., and P. J. Smith, "Mixing and Gasification of Coal in Entrained Flow Systems," ERDA Rpt., FE-2666-f, **2**, (1979).
Sprouse, K. M., "Modeling Pulverized Coal Conversion in Entrained Flows," *AIChE J.*, **26**, 964 (1980).
Szekely, J., J. W. Evans, and H. Y. Sohn, *Gas-Solid Reactions*, Academic Press (1976).
Thring, N. W., and R. H. Essenhigh, *Chemistry of Coal Utilization-Supplementary Volume*, H. H. Lowry, Ed., Chap. 17, John Wiley & Sons (1963).
Ubhayaker, S. K., D. B. Sticker, and R. E. Gannon, "Modeling of Entrained Bed Pulverized Coal Gasifiers," *Fuel*, **56**, 281 (1977).
Wen, C. Y., "Noncatalytic Heterogeneous Solid Fluid Reaction Models," *Ind. Eng. Chem.*, **60**, No. 9, 34 (1968).
Wen, C. Y., and E. S. Lee, Eds., *Coal Conversion Technology*, Addison Wesley Publishing Co. (1979).
Wen, C. Y., and L. T. Fan, *Models for Flow Systems and Chemical Reactors*, Marcel Dekker, New York (1975).
Wen, C. Y., and T. Z. Chuang, "Entrainment Coal Gasification Modeling," *Ind. Eng. Chem. Process Des. Dev.*, **18**, 684 (1979).
Zahradnik, R. L., and R. J. Grace, "Chemistry & Physics of Entrained Coal Gasification," *Adv. Chem. Ser.*, **131**, 126 (1974).

Manuscript received February 17, 1982; revision received January 7, and accepted February 28, 1983.

Decomposition of Systems of Nonlinear Algebraic Equations

MORDECHAI SHACHAM

Department of Chemical Engineering
Ben Gurion University of the Negev
Beer Sheva, Israel

A new method for decomposing irreducible subsets, in the solution of systems of nonlinear algebraic equations, is presented. This method consists of two steps: (1) elimination of the nonlinearity from some of the equations by replacing nonlinear expressions by new variables; and (2) formulation of a problem of smaller dimension by tearing the linear subset of equations. It is shown that these modifications do not change considerably the convergence rate of the Newton-Raphson and Broyden's methods while reducing the problem's dimension. Computer time reduction up to 80% is demonstrated in the examples solved. An algorithm for elimination of nonlinear expressions, which uses Boolean matrices instead of formula manipulation, is also presented.

SCOPE

Steady-state simulation or design of chemical processes gives rise to the need of solving large sets of nonlinear algebraic equations. In the equation-oriented flowsheeting programs which are currently being developed (Shacham et al., 1981), these may be problems containing tens of thousand of linear and nonlinear equations. The simultaneous solution of such a large number of equations is very time-consuming and may be even impractical. Fortunately, large systems of equations tend to be sparse so that each equation usually involves a small number of variables. This sparsity makes it possible to decompose the large system into a set of smaller problems which can then be solved sequentially. This process (usually denoted partitioning) decomposes the system into "irreducible subsets" which cannot be further partitioned. It has been proved that it is advantageous to partition a system to irreducible subsets (Hernandez and Sargent, 1979), and there are several algorithms available for partitioning.

Irreducible subsets can further be decomposed by "tearing." This operation reduces essentially the dimension of the irreducible subset, by selecting some of the variables as "tear variables" and expressing the additional variables in the subset as explicit functions of the tear variables. There are several difficulties in applying tearing techniques to nonlinear systems, the major ones being: (1) tearing requires formula manipulation which is very expensive in terms of computer time; and (2) the smaller system generated by tearing tends to be more nonlinear and more difficult to solve (Mah, 1972).

In this paper a new tearing method for systems of nonlinear equations is presented. This method does not require formula manipulation, and it either improves or does not change the convergence rate when the Newton-Raphson or Broyden's methods are used for solution.

CONCLUSIONS AND SIGNIFICANCE

The proposed tearing method includes the following steps:

1. Some of the nonlinear equations are linearized by replacing nonlinear expressions by new variables, and by adding new nonlinear equations to the system. The nonlinear expressions for replacement are selected so that the net effect of each replacement is reduction of the number of nonlinear equations in the system. The operations of this step are carried out in a Boolean matrix so that no formula manipulation is required.
2. Tearing of the linear subset of equations is carried out by using partial Gauss elimination in this subset to express all the variables as explicit linear functions of the tear variables. The number of the tear variables is equal to the number of the remaining nonlinear equations. It has been proved that these operations do not change the convergence rate of the Newton-Raphson method. Numerical experiments have shown that they may slightly improve the convergence rate of Broyden's method.

The net effect of the tearing is reduction of the dimension of